SEVERAL NOVEL APPLICATIONS OF MICROWAVE INTERFEROMETRY IN THE MEASUREMENT OF SOLID ROCKET PROPELLANT REGRESSION RATES

by

Daniel J. Klinger

A Thesis

Submitted to the Faculty of Purdue University

In Partial Fulfillment of the Requirements for the degree of

Master of Science in Aeronautics and Astronautics

Gambaro School of Aeronautics and Astronautics

West Lafayette, Indiana

August 2022

THE PURDUE UNIVERSITY GRADUATE SCHOOL
STATEMENT OF COMMITTEE APPROVAL

Dr. Steven Son, Chair

School of Mechanical Engineering

Dr. Alejandro Strachan

School of Materials Engineering

Dr. Terrence Meyer

School of Mechanical Engineering

Approved by:

Dr. Gregory Blaisdell

Dedicated to:

My parents, Marcella and Jeff

ACKNOWLEDGMENTS

I would like to thank my advisor, Dr Steven Son, as well as research faculty Tim Manship, for their guidance and shared expertise throughout the process of obtaining my Master's degree. I would also like to thank Gus Caito and Tim Wagner, whose hard work allowed the research program to advance as far as it did.

This research was developed with funding from the Defense Advanced Research Projects Agency (DARPA) under contract HR00112120005. The views, opinions, and/or findings expressed are those of the author and should not be interpreted as representing the official views or policies of the Department of Defense or the U.S. Government.

Research into the "Pintle Motor" discussed was made possible with the assistance of Valley Tech Systems, Inc. Descriptions and figures involving the Pintle Motor are used with permission.

TABLE OF CONTENTS

LIST OF TABLES

LIST OF FIGURES

ABSTRACT

When characterizing a new solid propellant, one of the most important steps in determining its usefulness is discovering how the burning rate changes in response to changes in pressure. While there are many dynamic methods for directly measuring the regression rate of a burning propellant sample, few of them are capable of being used in typical harsh motor conditions: high pressures, high temperatures, and in an environment comprised of propellant exhaust products. This paper describes and evaluates the use of two custom-built microwave interferometers, one operating at 35 GHz and the other operating at 94 GHz, in several different configurations for the measurement of propellant regression rates. Four different configurations of interferometer and waveguide are presented and contrasted, with example results of experiments included. A polytetrafluoroethylene (PTFE) waveguide, utilized in previous works for explosives detonation velocity characterization, was used to directly couple interferometer signal with a burning propellant strand. This PTFE coupling is shown to be applicable to pressure vessel studies by simply using a cable feedthrough. In this configuration, signal quality is high but signal amplitude is low, especially when the waveguide is encased by support structures. A novel PTFE truncated cone waveguide expander is presented which performs three tasks: expanding the microwave signal such that an oversized (relative to signal wavelength) strand may be examined via microwave interferometry, functioning as a weak antenna that can observe phenomena through interstitial material without picking up significant amounts of environmental reflection, and acting as a sealing surface for pressure vessel experiments. Additionally, the use of a more-standard hollow-core waveguide and high-gain antenna is displayed, highlighting the increased signal strength but the larger number of spurious reflections in the signal. This study shows, through various experiments using the aforementioned configurations, the capability of microwave interferometry to quickly characterize a full propellant burning rate curve using a single dynamic-pressure test with 40g of propellant in a 2.5cm diameter propellant strand. Several novel combinations of mechanical configuration and propellant composition are shown that may guide future studies into the use microwave interferometry for solid propellant regression rate analysis.

1. INTRODUCTION

One of the most important steps in evaluating a new solid propellant formulation is to measure the response of its regression rate (burning rate) to chamber pressure. In most solid composite propellants, the burning rate follows Saint-Robert's Law, $r_b = aP^n$, where r_b is burning rate, P is the bulk chamber pressure, a is the burning rate prefactor, and n is the burning rate exponent. Generally, the constants of this equation are found by performing several strand-burn experiments at a range of different pressures and then using that data to correlate the nominal burning rate with pressure. Most methods are only capable of measuring the average burning rate of a propellant at a single pressure per experiment.[1,2] Closed-bomb pressure analysis, pressure vessel break wire timing analysis, and various video and laser-based analysis methods exist, but they are all limited by their inability to measure burning rates with high temporal and spatial accuracy over a large pressure sweep in a single test. Several methods, such as ultrasonic measurement, real-time x-ray imaging, and microwave interferometry (MI) can potentially overcome these drawbacks; each method has its own use cases.

MI has been studied since the 1950s as a method for measuring the burning rate of propellants and detonation velocity of explosives.[3–7] MI is a non-intrusive, non-visual measurement technique that allows for high-accuracy dynamic burning rate measurements in a variety of pressure environments. The MI method uses low-power microwave radiation that is split into a reference signal and a test signal. The test signal goes through a propellant and is reflected off the solid-gas interface, and possibly the ions in the flame, at the burning surface of the propellant sample.[8,9] While many using MI for explosives, such as Glancy et al., Bel'skii et al., and Vuppuluri et al.,[10–12] have theorized that the locally ionized regions from reactions are essential for reflection of the microwave signal, others, such as Aničin et al. and Bozic et al.,[4,13] have shown that in deflagration experiments the ionization of the flame front contributes negligibly to microwave reflection, if at all. The reflected test signal has a change in phase related to the distance it has traveled and the properties of materials it has traveled through. When electrically mixed with the reference signal, the test signal constructively or destructively interferes, depending on the distance of the reflecting surface. A continually moving reflective surface creates a sinusoidal fringe pattern, with a frequency, f_s, proportional to the speed of the moving reflective surface and

the interference wavelength, λ_g, of the material it passes through. The frequency of the fringe pattern and the interference wavelength can be correlated with the burning rate, r_b, via

$$r_b = \frac{f_s \lambda_g}{2}. \quad (1)$$

As the frequency of a signal is related to the angular velocity, and therefore the time derivative of the signal's phase, by $2\pi f = \omega = d\phi/dt$, the relation can also be expressed in terms of the phase of the signal as

$$r_b = \frac{\lambda_g}{4\pi} \frac{d\phi}{dt}. \quad (2)$$

Derivations of Eq. 1 and Eq. 2 can be found in works by Kerns and Dayhoff,[3] Zarko et al., [14] and Renslow.[15] It should also be noted that this interferometry analysis is equivalent to analyzing the beat frequency of the wave superpositions as the change in frequency due to a Doppler shift from the regression rate of the burning surface. More detailed explanations of this equivalence may be found in Appendix B of a work by Cole (1965).[16]

The frequency of the fringe pattern can be analyzed through various methods, with advantages and disadvantages for each. Methods such as peak-picking, short time Fourier transforms, and Gabor wavelet transforms are discussed in detail by Kittel et al.[17]

Both interferometers considered in this paper also include a quadrature mixer, where one reference signal is 90° out of phase from the other. Both an in-phase and quadrature return signal are output, which allows for the computation of phase via an inverse tangent, with the continuous derivative of phase found by quadrature unwrapping and numerical differentiation. Quadrature unwrapping methods and mathematical corrections for common issues can be found in works by Kittel et al.,[17] Sur et al.,[18] and Heydemann.[19]

In this work, our objectives were to demonstrate and evaluate the effectiveness of microwave interferometry in a variety of material and pressure conditions using several microwave interferometer configurations and signal analysis methods. Additionally, an aim was to contrast the relative merits of each configuration and present example results of selected experiments.

2. METHODS

2.1 Propellant Properties.

The burning rates calculated by Eq. 1 and Eq. 2 are directly proportional to the interference wavelength, λ_g. Therefore, accurate determination of this constant is essential. The interference wavelength of the sample depends on the frequency of the probing interferometer, as well as properties of the propellant such as chemical constituents, strand shape, strand size, and material temperature. Direct measurement of this wavelength can be time and cost prohibitive as it commonly requires the use of a Vector Network Analyzer and careful sample preparation.[20,21] More rudimentary direct measurement of this constant can be performed by using video or break wire methods to accurately measure the time it takes the propellant to burn a precisely measured distance, and then correlating that with the MI frequency. This method requires destructive testing of multiple samples and setup for the calibration. However, if electrical properties of the propellant are known then the interference wavelength can also be calculated by

$$\lambda_g = \frac{\lambda_0}{\sqrt{\epsilon_r - \left(\frac{\lambda_0}{\lambda_c}\right)^2}}, \qquad 3$$

where λ_0 represents the wavelength in air at the MI operating frequency, λ_c represents the cutoff wavelength of the waveguide mode, and ϵ_r is the relative permittivity of the regressing material.[22] For a circular waveguide with radius *r*, the cutoff wavelength can be calculated by $\lambda_c = 3.41r$.[22] The relative permittivity of a material can either be directly measured or calculated from the measurements of individual species within a mixture. The basis for finding the relative permittivity of a mixture of two materials was first described by Landau and Lifshitz in 1960.[23] However, there were limiting assumptions that were removed in a 1965 publication from Looyenga that proposed a more general equation.[24] Despite the generalities developed by Looyenga, the application of the mixing relationship, $\epsilon_r = \left[\left(\epsilon_a^{1/3} - \epsilon_b^{1/3}\right)V_a + \epsilon_b^{1/3}\right]^3$, to the propellant samples generated for this study requires several simplifying assumptions to be made. Here ϵ_a and ϵ_b represent AP and HTPB, respectively, and V_a represents the volume fraction of AP within the propellant. The propellant is assumed to be a mixture of AP/HTPB, excluding all other additives, and to be free of any voids.

The relative permittivities for AP and HTPB-laden material were found in the literature to be 5.1[125] and 3.5,[26] respectively. The AP volume fraction was determined to be approximately 70% based on solids loading and density estimates for the average sample tested in this study. This produced a relative permittivity estimate of $\epsilon_r = 4.58$, which was used for all propellant samples. The assumption of a simple AP-HTPB system is not entirely valid for highly aluminized propellants and adjustments should be made for propellants which contain significant amounts of other additives.

2.2 Research Propellants Preparation.

For the various experiments discussed in this paper, the typical research propellant composition was the oxidizer ammonium perchlorate (AP, procured from Rocket Motor Components, or RCS) formulated with a hydroxyl-terminated polybutadiene (HTPB, RCS) binder. Either modified methylene diphenyl diisocyanate (MDI, RCS) or isophorone diisocyanate (IPDI, procured from TCI America) was used as a curative. Tepanol (HX-878, procured from CRS Chemicals) or Aziridine (HX-752, procured from Mach I Chemicals) was used as a bonding agent. Isodecyl pelargonate (IDP, RCS) was used as a plasticizer. Formulations on occasion contained triphenyl bismuth (TCI Chemicals) as a cure catalyst, and various sizes of aluminum (procured from Valimet) or iron oxide powder (RCS). Research propellant solids loading was 70-88%.

Most research propellant strands were mixed with a resonant acoustic mixer, LabRAM II, produced by Resodyn Inc., however some were mixed using a 1-qt Ross dual planetary mixer or a 20-qt Hobart planetary mixer. Research propellant strands were cast into low-density polyethylene (LDPE) cylinders of about 7.2mm inner diameter, larger (25-32mm diameter) LDPE cylinders, G10 Garolite cylinders, and paper phenolic tubes. Each research propellant grain was trimmed, using various methods, to achieve a high degree of flatness. This process aided in maintaining a flat burn surface throughout the entire burn.

During experiments, research propellants were inhibited to prevent side burning and create as flat of a burning surface as possible to avoid complex microwave reflection. Typically, research propellants tested at atmospheric pressure were burned in the LDPE tubes that they were cast into. The LDPE burns away slowly with the research propellant and leaves very little residue. Most

[1] Refractive index is given in the cited work. Relative permittivity ϵ is related to refractive index in non-magnetic materials by $\epsilon = n^2$

pressure vessel experiments used one or more coats of nail polish. Before burning, the ethyl acetate of the nail polish inhibitor is dried, leaving behind a thin, minimally intrusive butyl acetate/nitrocellulose inhibitor. Several other experiments were inhibited with more regression-resistant materials, such as the G10 Garolite casting cylinders, or thick coats of various epoxies.

2.3 Microwave Interferometer Operation.

Two custom-built microwave interferometers were used for experiments. The 35 GHz interferometer, shown in Figure 2-1, was built by Electrodynamic of Albuquerque, NM. It uses two oscillator sources, an 8 GHz source at 20dBm and a 27 GHz source at 17dBm, which are mixed to produce an output signal of 35 GHz at 2.5dBm. The system outputs the interferometer return signal mixed with both an in-phase (0° phase offset) and a quadrature (90° phase offset) reference signal as separate channels. The two-channel output allows for quadrature-based phase calculation as well as determination of direction of regression measured by the interferometer. A diagram of the interferometer internals is shown in Figure 2-2. The microwave output is a rectangular WR-28 waveguide with a UG-599 flange that can be connected to other waveguides/microwave components as needed.

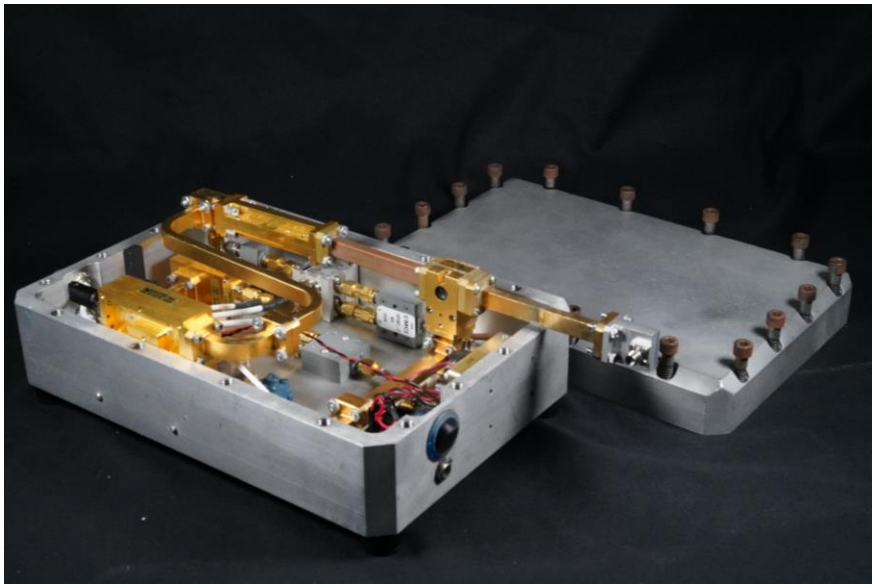

Figure 2-1: 35 GHz Microwave Interferometer with top cover removed.

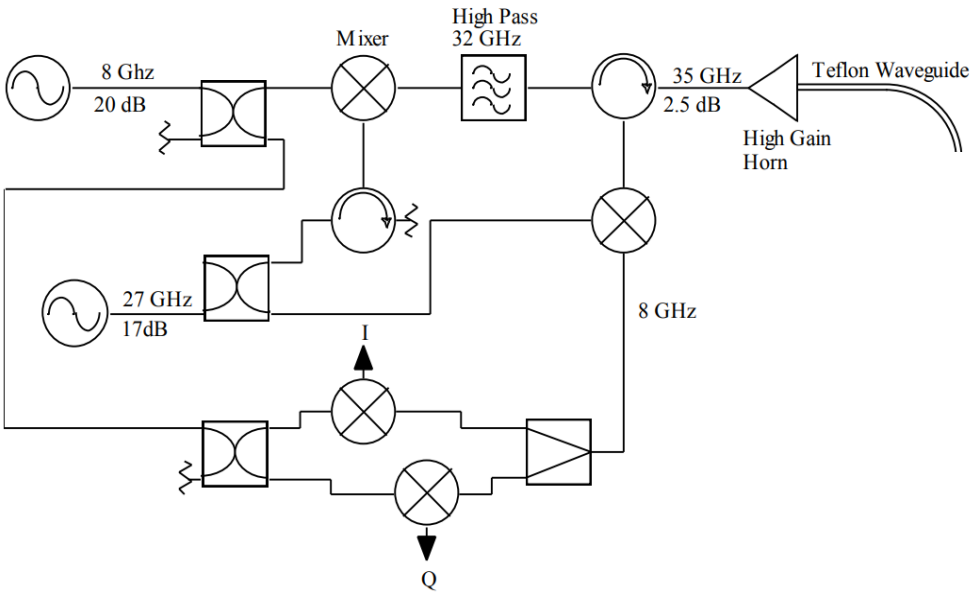

Figure 2-2: 35 GHz microwave interferometer diagram.[15]

The 94 GHz interferometer operates using the same principles as the 35 GHz interferometer. The interferometers are of similar power and deliver similar output voltages for both in-phase and quadrature channels. The microwave output is a rectangular WR-10 waveguide with UG-387 flange that can be connected to other waveguides/microwave components as needed.

The interferometers were typically used with shielded coaxial cables attached to a Tektronix DPO4034 Digital Phosphor Oscilloscope for data collection. Collected interferometry signals had an amplitude on the order of 1-5mV, although the DC offset of the signal was several dozen mV, and the DC offset drifts as the interferometer warms up. The MI signal position on the oscilloscope screen was checked before every test to ensure that the signal had not drifted beyond recording limits. Typical sampling rate used was 2.5 kHz, though for some experiments, up to 50 kHz was used. Interferometer response fringe frequencies were on the order of 0.5 – 30 Hz, so this sample rate is more than sufficient to capture wave properties. Both interferometers have an output power of about 1 dBm, which is low enough that propellant heating and exposure to test personnel is not a concern.

Using Eq. 3 and constants described above, the propellant interference wavelength for a sample 7mm AP-HTPB composite propellant strand was calculated for each interferometer and is shown in Table 1.

Table 1: Interference Wavelength of a sample AP Composite Propellant at Different Microwave Frequencies.

Microwave Frequency (GHz)	Free-Space Wavelength (λ_0, mm)	Interference Wavelength (λ_g, mm)
35	8.56	4.25
94	3.15	1.48

2.4 Support Equipment Description.

For all experiments performed, analog MI data was recorded using a Tektronix DPO4034 Digital Phosphor Oscilloscope operating in 50Ω resistance mode (low resistance) and high-resolution mode (50 MHz low-pass filtered). Sampling rates were between 2.5 kHz and 50 kHz. These recording rates were more than sufficient to measure the MI signals of between 0.4 and 40 Hz. High-speed visual recording was performed using either a Phantom V5 or Phantom V10 high speed camera. Low-speed validation recording (up to 120 fps) was performed using a Sony A7 II DSLR.

2.5 Microwave Interferometry Experiments.

Typical experimental configurations considered are shown in Figure 2-3. These configurations will be referred to as A, B, C, or D configuration, as indicated in Figure 2-3.

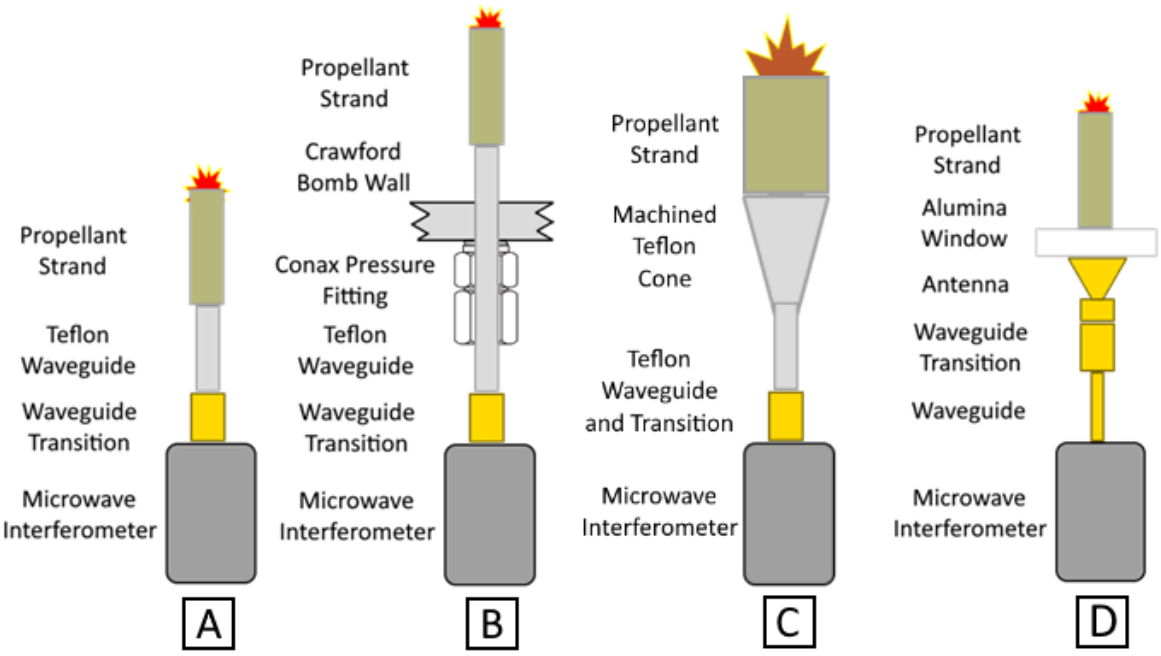

Figure 2-3: Typical microwave interferometer configurations. From left to right: A) With PTFE waveguide, B) Strand tests in pressure vessel, C) With machined PTFE waveguide expander, D) With antenna and microwave window.

The A configuration was used for atmospheric tests. In this configuration, a rectangular-to-circular waveguide transition was attached to the end of the microwave interferometer, and a Polytetrafluoroethylene (PTFE) waveguide was inserted snugly into the transition (7mm diameter for 35 GHz, 2mm diameter for 94 GHz). The microwaves travel through the PTFE and into the propellant strand. The propellant strand was then mechanically connected to the PTFE, typically by a small roll of electrical tape attaching the propellant to the PTFE. A 3D printed PLA structure was used to direct the waveguide.

The B configuration represents a simple way to measure strand regression rate in a pressure vessel. With this method, a PTFE rod was sealed into a PG2S-250-A-L Conax pressure fitting with LAVA non-conductive crush sealant material and threaded into an appropriate port on a pressure vessel. However, it should be noted that the Conax fitting was not tightened according to specification, as the PTFE waveguide would shear if too much force was applied. Therefore, the fitting is likely not capable of withstanding the rated 69 MPa of pressure listed on the Conax manual. A propellant strand was then attached to the PTFE in the same manner as configuration A and a burn test performed at pressure.

The C configuration is modification on the A or B configuration for use with propellant strands of much larger diameters (tested with 25mm and 32mm diameter strands, 25mm long). The C configuration can be used in pressure vessels, where it dispenses with the Conax pressure fitting by using a PTFE truncated cone as the main sealing surface. Additionally, a thin (3.2mm) alumina disk was placed between the PTFE horn and propellant strand and the edges of the disk sealed with epoxy to prevent reliance upon the PTFE for sealing pressure. The cone was lathed from 32mm diameter PTFE round stock to a larger diameter of 25mm and a smaller diameter of 9.5mm, with a 12.5° half-angle. This angle was chosen as a shallow angle for the signal to turn. The PTFE waveguide was inserted snugly into a 13mm deep hole drilled on the small side of the cone to couple the microwave signal from the waveguide to the cone transition.

The D configuration utilizes a hollow-cored WR-10 or WR-28 waveguide was connected to a medium/high gain antenna. For the experiments discussed, an Erevant SAC-1533-250-S2 15dBi medium-gain antenna was used for the 35 GHz MI, and an Erevant SAC-2012-094-S2 20 dBi high-gain antenna was used for the 94 GHz MI. Additionally, as the hollow-core waveguide is very rigid, a microwave-compatible high-frequency coaxial cable was often used instead to allow for more dynamic mechanical setups, despite thee coaxial cable having more signal loss per unit distance. In this configuration, alumina windows were used to protect the antenna from heat and propellant exhaust products, as well as to separate pressurized space from unpressurized space. Alumina is typically used in MI applications due to its high transmittance to microwave radiation. Other possible materials window materials include sapphire glass, boron nitride, and aluminum nitride.[27]

2.6 Fringe Pattern Analysis.

Once an MI experiment has been conducted, the signal is analyzed to determine the burning rate. Generally, there are two types of analyses that can be performed: discrete and continuous. Discrete analyses take in a significant portion of a waveform and return a frequency only for that section. This gives a temporal resolution near the period of the signal (around 0.2 – 2s). Continuous analyses can give a temporal resolution nearing the sampling rate, rather than the signal frequency (~1 ms resolution). A typical signal pattern of a non-metallized 7mm sample in configuration A, normalized such that signal mean is around 0, is shown in Figure 2-4. As shown, these signals are sinusoidal, at an approximately constant frequency indicating a nearly constant burning rate. The

quadrature channel is 90° ahead of the in-phase channel, as designed. Additionally, signal magnitude increases as time goes on because the sample is becoming shorter and therefore there is less propellant to decrease the signal amplitude via absorption and scattering on small voids and other propellant inhomogeneities. The instantaneous burning rate can be found using either Eq. 1 or Eq. 2, presented in the introduction. However, determining the instantaneous frequency or phase derivative is non-trivial. As discussed in the introduction, Kittell et al. provide an overview of several methods of analysis.[17] Additionally, several improvements and brief descriptions of methods used to calculate burning rate are presented below.

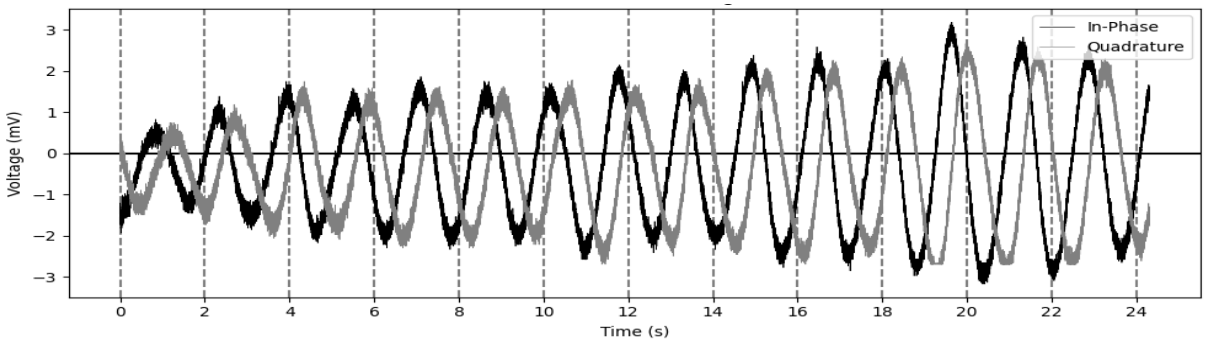

Figure 2-4: Typical MI response for atmospheric strand burn.

2.6.1 Discrete Methods of Fringe Pattern Analysis

One method that was used to measure MI fringe frequency was peak picking, which is the simplest approach. In this method, an automated routine was used to find the local minima, maxima, and zero crossings of each period of the signal. With the time that the i^{th} minima, maxima, or zero crossing occurs as t_i, the frequency of a quarter period is found as one quarter of the inverse of $t_{i+1} - t_i$. To help improve measurement accuracy, the signal was zero-phase band-pass filtered to remove noise as well as DC offsets, while preserving the temporal location of frequency information. In constant pressure strand burn experiments, the average frequency was used to determine the burning rate. To correlate a burning rate with other sensor equipment in dynamic burning rate experiments, the time a frequency occurred at was said to be the average of t_i and t_{i+1}. A 4-point rolling average was typically used to smooth the transient frequency response. The temporal resolution with this approach, however, is limited based on the frequency of the response signal.

2.6.2 Continuous Methods of Fringe Pattern Analysis

Typically, when time-precision of greater than ¼ fringe wavelength is needed, a quadrature-based phase analysis is performed to get the instantaneous phase of the signal, and then a numerical derivative is taken to get the phase derivative for use in Eq. 2.[17] Various corrections are then used to remove errors in interferometer and experimental setups.[19] This method has been shown to be effective for well-behaved explosive measurements.[12,17] However, in propellant strand burn experiments, issues such as single-channel nonlinear drift, loss of coherence, and mode changes made these corrective measures often fail to resolve a clear signal. This causes the tangent of the two signals to change unpredictably in ways not observed in the actual burning rate.

For this reason, a simpler method of finding the signal phase, and therefore the phase derivative, was to take the arcsine of each signal individually. However, arcsine only correctly gives the phase on signals that go from exactly -1 to 1, while experimental signal magnitudes vary greatly, so the signal must be normalized first. This normalization was performed by first band-pass filtering the signal to remove any high-frequency noise, DC offsets, and low-frequency effects like linear magnitude shifts. The signal was then divided by the magnitude of the sum of the signal and its Hilbert transform at all points. As the Hilbert transform is the purely imaginary 90° phase-shifted complement of the signal, the instantaneous magnitude of the signal can be found from the sum of the original signal and its Hilbert transform. Taking the arcsine, a piecewise discontinuous function is obtained, as the sign of the derivative changes at local minima and maxima. Next, a numerical derivative is taken of the phase, and the absolute value is taken to get a continually positive burning rate. The discontinuities at the extrema of the signal can be lessened by taking a rolling average or using a linear interpolation for a set number of points on either side of a peak. This approach is expressed as $r_b = \frac{\lambda_g}{4\pi}\frac{d\phi}{dt} = \frac{\lambda_g}{4\pi}\left|\frac{d}{dt}\left[\arcsin\frac{v(t)}{|v(t)+Hilb(v(t))|}\right]\right|$, where $v(t)$ is the band-passed signal voltage at time *t*, and $Hilb(x(t))$ is the Hilbert transform of a signal *x(t)*. The derivative of phase is found by using numerical finite differencing methods or Fourier-domain filtering techniques.

Another single-phase method of analyzing the MI signal frequency is to use various Fourier filters and arctangent analysis in order to determine the instantaneous phase derivative at any point in the signal. This method is more reliable than the arcsine method as it less susceptible to noise and signal compression near the minima and maxima of the sinusoidal pattern. In this method,

similar to the previous method, a Hilbert transformer is used to create a signal which is 90° offset from the original signal. Then, the instantaneous phase is calculated simply by taking the arctangent of the two signals. The derivative of the phase is found similarly by finite differencing or Fourier-domain filtering methods.

2.7 Experimental Setup.

Unless otherwise specified in the results section, experiments were performed with the MI in one of the simple configurations described above: either A configuration for atmospheric pressure tests or B configuration for Crawford Bomb pressure vessel tests. However, several experimental setups shall be discussed in detail.

One such testing format that will be presented is the coherence depth testing setup, shown in Figure 2-5. This test setup uses the D configuration, described previously, with a 9.5mm thick alumina disk (99% purity from AdValue Technology) and an Aramid and epoxy-based insulator separating the propellant from the horn antenna. This setup was intended to mimic the mounting and microwave transmission environment of future transient-burn testing. When the burning surface is far from the antenna, multimode and multi-reflection interference cause a malformed sine wave to form that is not entirely representative of burning rate. As the propellant regresses, a "coherent" sine wave forms.

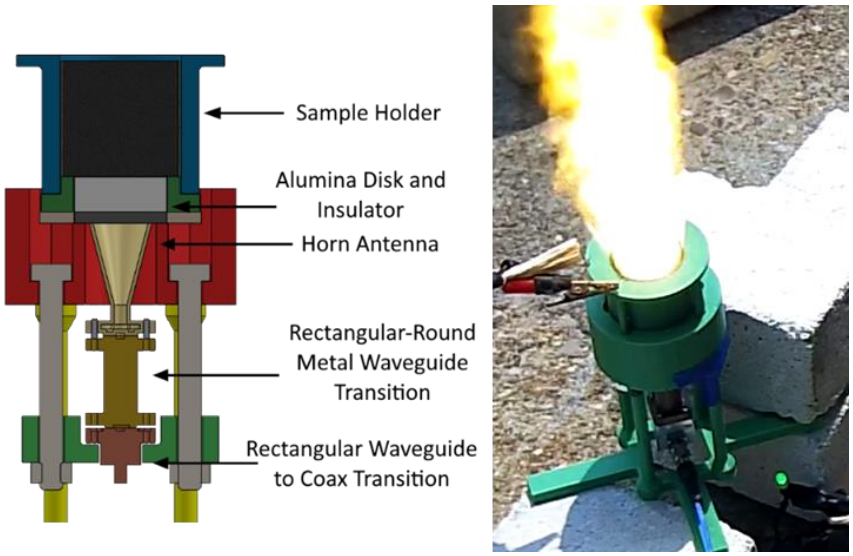

Figure 2-5: Coherence depth testing setup diagram (left) and test fire (right).

Another test format discussed is that of the dual-propellant pseudo-motor. A cutaway diagram of the MI interface in this experiment is shown in Figure 2-6. As shown, the propellant regression rate is measured using configuration D, with the 9.5mm thick alumina window acting as a sealing surface in conjunction with an O-ring along the circumference of the disk. This experiment was performed with both the 35 GHz and 94 GHz microwave interferometers. In this experiment, a gas-generating center-perforated "driver grain" provides a motor-like environment that a "target grain" experiences and burns in. The pressure, temperatures, and gas composition experienced by the target grain should be very similar to that of actual rocket motor conditions, giving a more accurate representation of true propellant burning rate than a closed bomb strand test while using less test propellant than a series of full-size motor tests. The driver grain is designed to produce a progressive burn, so that the MI observes the target grain regression rate in a varying pressure environment. The MI measurements are synchronized to a pressure transducer data acquisition system elsewhere in the experimental setup via a 24V relay, and therefore the instantaneous burning rate of the propellant can be plotted as a function of pressure. This enables a burning rate curve to be derived from very few, or a single, experiment using approximately 40g of target propellant. This test format was designed to approximate propellant conditions and mechanical mounting of another experiment: the "pintle motor", described below.

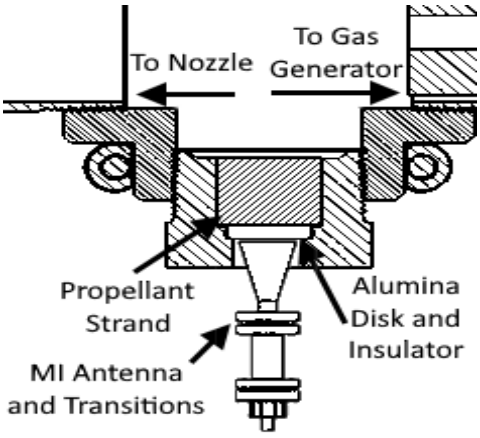

Figure 2-6: Dual-propellant pseudo-motor setup diagram.

Many of the aforementioned experiments were in preparation for transient pressure experiments in the pintle motor configuration. This experiment, using proprietary hardware and software from Valley Tech Systems Inc., uses a 30-40g target propellant grain to pressurize a small

combustion chamber with a variable-area nozzle throat in order to tightly control chamber pressure. The target grain is set in a plug with very similar configuration to Figure 2-6, with the target grain up against an alumina microwave window on one side and exposed to motor-like combustion gasses on the burning side. The 9.5mm thick alumina disk seals against an O-ring to hold pressure. Beyond the propellant grain is a plenum designed to be long enough to allow for complete combustion of aluminum in the propellants, followed by a variable-area nozzle throat. The area of the nozzle is controlled by a pintle whose depth in the throat is changed rapidly by a pressure controller in order to maintain the desired pressure profile. All experiments involved a hold at 13.8 MPa, followed by a controlled linear depressurization to 3.4 MPa, and a hold at 3.4 MPa until the propellant was exhausted.

3. RESULTS

3.1 MI Configuration Comparison.

The various configurations discussed previously each have benefits and drawbacks to their use. Some were used for small-diameter propellants, while others were used for large-diameter. The environment around the propellant needed to be taken into account before a method was chosen for an experiment, as well as the pressure environment that it would experience. Mechanical constraints and expected signal quality were also taken into account to determine what configuration was most appropriate for each experiment performed.

The A configuration is desirable as all microwave radiation that is not lost along the PTFE waveguide is transmitted directly into the propellant. The waveguide only picks up reflections from a very narrow cone opposite the waveguide and the microwave signals are reduced in amplitude by the low transmittance of the propellant such that reflections from environmental objects are not picked up. The A configuration is less desirable in that only small-diameter propellants can be tested accurately and mechanical alignment/coupling is more difficult due to the tendency of significant mechanical restraint to weaken the signal to non-usability.

Signal strength is reduced in a variety of ways in this setup. First, the length of PTFE is inversely proportional to the amount of return signal. PTFE is not a perfect waveguide and thus has distance-related losses. Second, the length of propellant, flatness of burning surface, and flatness of mating surface are essential factors in receiving a high-quality reflected signal. Finally, an object in contact with the PTFE reduces this signal strength as well. An in-depth analysis of this mechanism has not been performed, but certain materials degrade the signal to a greater extent, and the tighter the PTFE is gripped over more surface area, the more signal is lost.

In the B configuration, behaving similarly to the A configuration, compression of the PTFE and proximity to metal fittings reduces the amplitude of signal visible at the oscilloscope. However, the frequency content of the signal is maintained and with a high-precision analog-digital convertor and good noise rejection, the signal is still adequate with typical methods. This method is desirable for pressure vessel testing as it is robust, simple to set up, and uses a corrosion-resistant waveguide. In addition, the inability of the mated PTFE strand to pick up other reflections in the pressure vessel is a benefit of this method when compared to antenna-based method. However, the lower

signal amplitude can make it difficult to analyze signals. In addition, due to under-tightening of the Conax fitting, the actual strength of the seal is not none. One failure of the pressure seal occurred during testing at ~15.2 MPa. However, prior and subsequent tests at higher pressures show that this may have been an isolated incident.

In the C configuration, the 25mm PTFE cone has much better mechanical contact with larger strands and also beneficially acts as a weak antenna: picking up reflected signal in a wider arc and at a longer distance than a straight PTFE waveguide. The C configuration was not used for small-diameter propellants because it is less directional than the B configuration. Additionally, this configuration was not used often for large diameter pressure vessel tests, as the D configuration was more reliable, mechanically sound, and produced a cleaner signal.

The D configuration is the most modular design and typically yielded the highest power available at the sensing end (more power is lost in PTFE waveguides due to dielectric effects). It is also desirable due to its ability to project a microwave signal further into a sample and its usage on larger diameter samples. Furthermore, no mechanical connection between the propellant sample and the alumina is needed. However, because the antenna is much more effective at projecting microwave energy, it can pick up spurious and misleading motion from the vibration of support equipment or multipath reflections in pressure vessels. In addition, sample preparation is more important with configuration D to ensure that mating surfaces and burning surfaces are very flat.

3.2 Sample Analysis of Steady-Burning Test.

Results from a strand burn test in a Crawford-style pressure vessel are shown below. In this test, a 30mm long, 6.3mm diameter strand of 18% H30 aluminum, 87% solids loading AP/HTPB propellant inhibited with two coats of nail polish was burned at 13.8 MPa. Configuration B, described in the experimental section, was used with a 35 GHz MI. A visual representation of the burn is shown in Figure 3-1. The burn was fairly planar and exhibited a near-constant burning rate, but it should be noted that the inhibitor did not burn away at the same rate as the propellant. The unburned inhibitor caused a small burning rate transient as the strand entered the inhibitor tube.

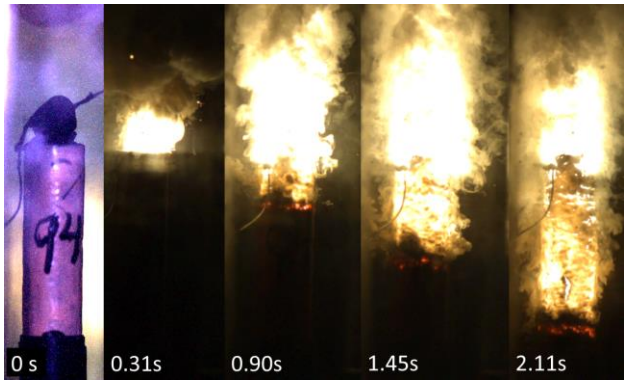

Figure 3-1: Visual time history of a propellant strand burn in a pressure vessel at 13.8 MPa.

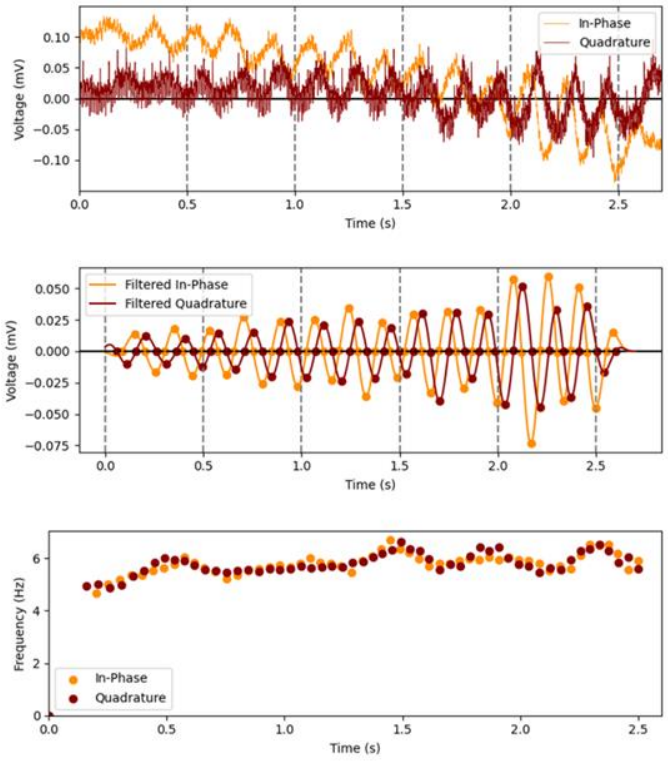

Figure 3-2: Unfiltered signal (top), filtered signal (mid), and resultant frequencies (bottom) from propellant strand burn in a pressure vessel at 13.8 MPa.

The raw trace from this experiment is shown in Figure 3-2. The signal voltage was very low, at less than 50µV peak-to-peak, resulting in a low signal to noise ratio. Also, the in-phase component exhibited drift in the DC offset over the course of the experiment. By using a 4th order Butterworth bandpass filter (forward and backward filtering to create a 0-phase filter), the central plot of Figure 3-2 was created. While the filtering created a usable signal for peak picking, the

signal was not strictly increasing in amplitude, as typically expected. This indicates either a mode shift of the microwave signal in the propellant sample or a change in the dominant reflective surface measured by the MI. An automated routine extracted the minima, maxima, and zero-crossings of the detrended sine wave. The bottom portion of Figure 3-2 shows the resulting frequencies, which are proportional to the burning rate by Eq. 1. The burning rate had a small startup transient as the strand burned into the tube formed by the unburned inhibitor, and was non-steady at the end, likely due to non-planar burning. There is agreement in the in-phase and quadrature signals for most of the burn, indicating a physical result from the data processing (as opposed to artifacts of data correction processes). There is a slight upward trend in the burning rate, likely because combustion gases caused chamber pressure in the closed bomb to increase from 14.1 MPa to 15.1 MPa over the course of the burn.

Power reflected from the solid-gas interface back to the MI during a burn is reduced due to absorption depending on the length of the propellant as well as from scattering due to metal particles and voids within the propellant.[3] Metal particles and voids suspended in the propellant also generate weak multi-path reflections to the burning surface, which can influence the dominant reflection signal in undesirable ways. An experiment with a low signal to noise is said to lose "coherence", and typically will do so at the beginning of a burn, when the waveguide or antenna is far from the burning surface. Using the experimental setup shown in Figure 2-5, the distance at which coherence begins was measured for different propellant formulations using the 35 GHz and 94 GHz MI setups. The results of performing this test on a lightly metallized propellant formulation (RCS Warp 9) are shown in Figure 3-3. By setting a threshold for signal self-similarity via auto-correlation, it is determined that 81% of the signal is "coherent". By assuming a constant burning rate on the 32.6mm long strand, a 26.4mm coherence depth is found for this propellant. This experiment was performed on a small matrix of propellant samples and the results are shown in Table 2.

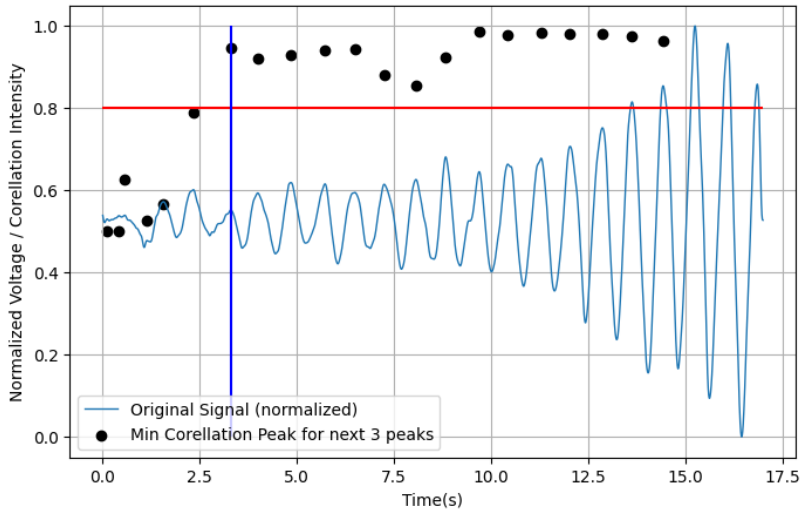

Figure 3-3: Autocorrelation analysis to test coherence depth.

Table 2: Coherence depth of different propellants and interferometers for a particular test setup.

	35 GHz MI	**95 GHz MI**
Lightly Metallized (~0.5% aluminum)	28.7mm	23.1mm
Highly Metallized (20% aluminum)	17.3mm	12.7mm

3.3 Sample Analysis of Burn-Rate-Sweeping Test.

Besides being a non-visual, non-intrusive measurement, another major benefit of using an MI system is the ability to measure and directly correlate the instantaneous burning rate of a propellant with pressure, temperature, and other propellant or chamber properties. Using the dual-propellant pseudo-motor experiment detailed previously, a trial was performed in which a progressive burn driver grain created chamber pressures ranging from 1.4 MPa to 11.2 MPa. The resulting fringe frequency vs time and a log-log plot of calculated regression rate vs chamber pressure are shown in Figure 3-4. The regression rate doubled over the course of the burn and was well-correlated with pressure. Performing a linear regression on the log of both instantaneous burning rate and pressure, the burning rate law determined for the propellant was $r_b = 0.115\ P^{0.274}\ in/s$ ($11.4\ P^{0.274} mm/s$ in SI). The propellant tested was RCS Warp 9, a non-metallized catalyzed propellant which is known to have burning rate parameters of

$a = 0.123 \frac{in}{s \cdot psi^n} \left(13.0 \frac{mm}{s \cdot MPa^n}\right), n = 0.287$,[28] so with a single test the error is 6.75% for a and 4.63% for n.

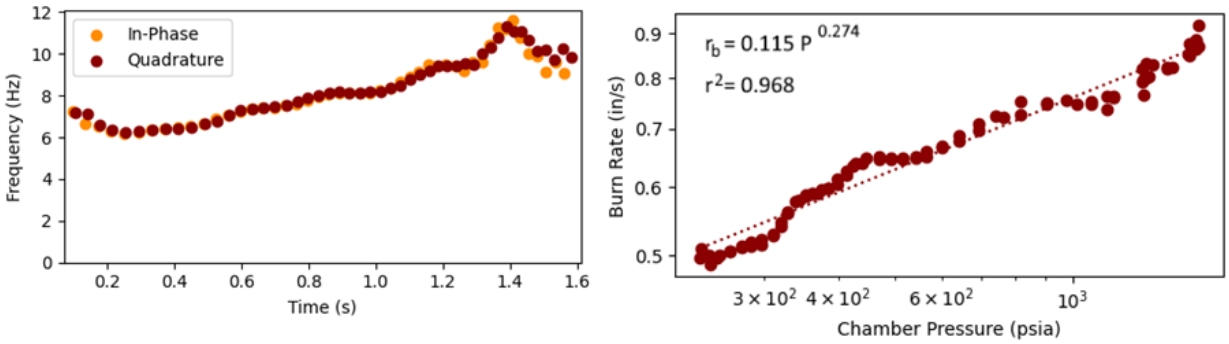

Figure 3-4: Burning rate of dual-propellant pseudo-motor for a non-metallized catalyzed propellant in uncorrected frequency (proportional to burn rate) vs time (left) and burning rate vs pressure log-log plot, with accompanying burn rate law in mm/s and MPa (right).

The microwave interferometer is also capable of resolving regression rates in conditions thought to be poorly suited for microwave interferometry. Shown in Figure 3-5, a test was conducted on an uninhibited 68.6mm long, 7.4mm square strand of an AP/HTPB propellant with 87% solids and 28% H30 aluminum content in test configuration A. The lack of inhibitor resulted in significant coning, which should cause a non-planar reflection of microwaves and thus poor resolution of burning rate. However, with the direct-contact waveguide, the reflected signal was still received (despite heavy attenuation from metal particles), and a true burning rate was resolved from the frequency of the fringe pattern using Eq. 1. The solid propellant has a higher bulk regression rate when it burns at an angle and thus the cone formation can be seen in the rise in signal frequency in Figure 3-5. While MI has been shown to be effective when surface curvature is much smaller than the interference wavelength by Strand et al.,[29] in this experiment the surface curvature is approaching the interference wavelength, and yet an accurate, coherent signal was able to be obtained. While the MI has not been observed to be able to resolve a coherent burning rate in all cases of coning, this example (and others not presented) show that it is capable.

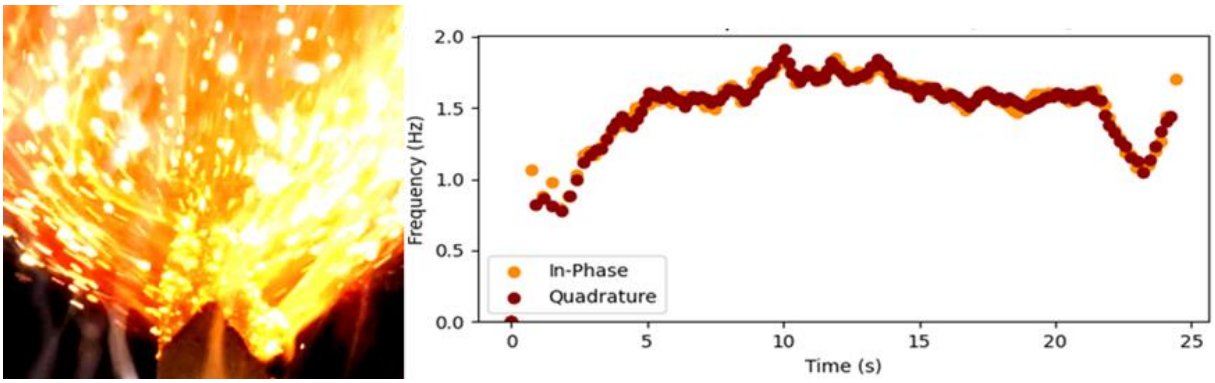

Figure 3-5: Image of burning highly metallized strand (left) and frequency response (right).

3.4 Sample Analysis of Pintle Motor Test.

With this controlled experiment, an entire burning rate curve from 3.4 – 13.8 MPa can be quickly obtained in a single test taking less than an hour. Unlike the dual-propellant pseudo-motor, the pressure profile is tightly controlled, such that multiple sets of test propellants can be evaluated using identical pressures conditions. In addition, the pressure profile may be adjusted as desired, to have a longer hold at higher pressure or a gentler slope towards low pressure, for example.

Due to the testing environment, the MI data collected tends to be high-noise, with peaks in noise amplitude near 30 and 60 Hz. Aggressive band-pass and notch filters therefore were needed in many runs of the experiment. In some cases, different band-pass filter limits were applied to different sections of the MI burn rate data. To aid in this process and collect the data most representative of real conditions, a Graphical User Interface (GUI) tool was developed to quickly change filter parameters, visualize data, and create burning rate-pressure correlations. A representative screenshot of this GUI can be found the Appendix. The GUI was also used to visualize any discrepancies between various discrete and continuous fringe pattern analysis methods.

A sample output a pintle motor test is shown in Figure 3-6. This highlights the precise control exerted over the pressure in the pintle motor. In most tests, the depressurization rate was 20.7 MPa/s. This shows that the MI is capable of measuring the burning rate over very high depressurization rates. In addition, from the high coefficient of correlation, the figure shows that the full burning rate curve can be determined with good certainty from only a single test. However, it should be noted that during the 3.4 MPa pressure hold, the burn rate did not remain entirely

consistent. It is predicted that this is largely due to non-planar burning in the large-diameter propellant samples as they burned down in their confiners.

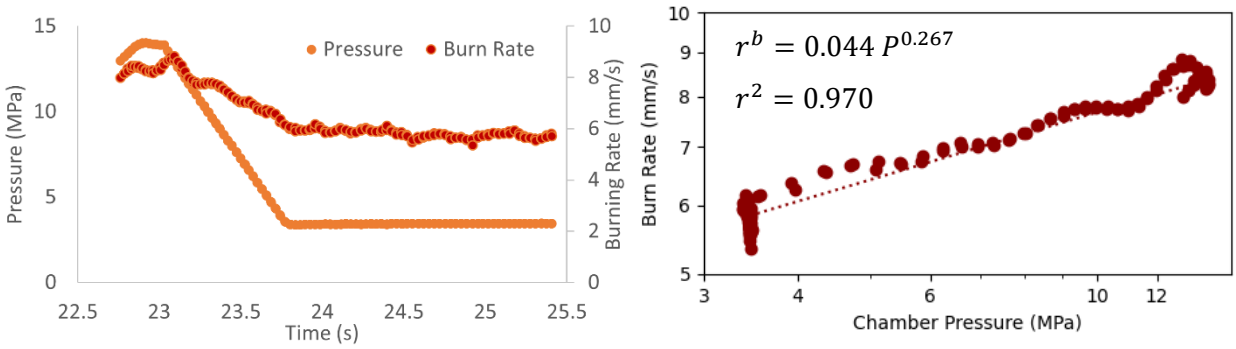

Figure 3-6. Burning rate and pressure trace of pintle motor test for an 82% solids loading, 5% aluminum sample (left) and burning rate vs pressure log-log plot, with accompanying burn rate law in mm/s and MPa (right).

4. DISCUSSION AND CONCLUSIONS

Several different configurations for using a microwave interferometer to measure propellant regression rates are presented, including a simple MI method for measuring the regression rate of a propellant in a pressure vessel. The use of microwave antennas to measure propellant burning rate is discussed, and examples of successful trials are presented. The ability of microwave interferometry to measure transient regression rates, as well as to correlate burning rate with pressure to get propellant properties, is demonstrated. An example of how certain configurations of a microwave interferometer can measure propellant regression in challenging conditions is shown. Robust methods for measuring the frequency and phase angle derivative of a microwave interferometer signal are described.

Of the configurations shown, configuration A is most useful when using strands of comparable diameter to the waveguide. The direct mechanical coupling also helps reject multipath reflections as this method has a very narrow beamwidth compared to configuration D. Configuration B is an extension of configuration A that can be used when the benefits of configuration A are desired in a pressurized environment. However, the pressure rating of this method was not firmly established above 13.8 MPa. Configuration B is an interesting new idea that can easily be incorporated in existing hardware for a Crawford-style strand burner or similar pressure vessel. Configuration C is an extension of configuration A that can be used with much larger diameter propellant strands. Configuration C is useful as it functions as a weak antenna: picking up reflections from further away than configuration A while rejecting multipath reflections better than configuration D. Another major benefit of configurations A-C is that the PTFE waveguide parts are significantly cheaper than hollow core waveguides and horn antennas and can more readily be considered consumable in the experimental setup.

The major benefit of configuration D is in correcting the main drawback of configurations A-C: power available at the sensor end. Configuration D is capable of penetrating thicker propellant strands because less microwave power is dissipated along the low-loss hollow-core waveguide and from mechanical restraint of the waveguide. Good filtering allows very weak return signals to be picked up in the other configurations, but internal reflections and scattering render the signal unusable in shorter lengths of propellant than configuration D. Furthermore, configuration D is more readily applied to high-pressure environments, as the only consideration

for its use is the structural integrity of the alumina window that faces the burning propellant, rather than sealing against the weaker PTFE waveguide.

Microwave interferometry is shown to be a useful method for the measurement of propellant regression rates in tasks where time-correlation is important, visual measurements may not be possible, and where propellant burning conditions may not be ideal. From the results of experiments such as the dual-propellant pseudo-motor and the pintle motor, it is shown that microwave interferometry is capable of quickly characterizing an unknown propellant's burning rate curve using a single dynamic-pressure test with 40g of propellant in a 2.5 cm diameter strand.

APPENDIX

ADDITIONAL FIGURES

Figure A - 1: Screenshot of the rapid analysis tool developed to aid in processing of pintle motor tests. The tool includes many useful features, such as the ability to rapidly change the start and end time of the signal under consideration, snapping the signal start to the pressure synchronization signal, rapidly changing filter cutoffs and parameters, and many other options. In addition, a Fast Fourier Transform (FFT) of the signal is shown to quickly gauge the major frequency content of the signal as a whole. Furthermore, there is another tab (not pictured) where the pressure trace can be loaded and quickly synchronized to the MI. On that window, a display of the pressure-burning rate graph is shown, and Vielle's Law parameters (with r^2) are shown for rapid analysis. The tool was written in Python 3 using PyQt5 and PyQtGraph libraries.

REFERENCES

(1) Gupta, G.; Jawale, L.; Mehilal; Bhattacharya, B. Various Methods for the Determination of the Burning Rates of Solid Propellants - an Overview. *Central European Journal of Energetic Materials* **2015**, *12* (3), 593–620.

(2) Zarko, V.; Kiskin, A.; Cheremisin, A. Contemporary Methods to Measure Regression Rate of Energetic Materials: A Review. *Progress in Energy and Combustion Science* **2022**, No. November, 100980. https://doi.org/10.1016/j.pecs.2021.100980.

(3) Kerns, D. M.; Dayhoff, E. S. Theory of Diffraction in Microwave Interferometry. *Journal of Research of the National Bureau of Standards Section B Mathematics and Mathematical Physics* **1960**, *64B* (1), 1. https://doi.org/10.6028/jres.064b.001.

(4) Bozic, V. S.; Blagojevic, D. D.; Anicin, B. A. Measurement System for Determining Solid Propellant Burning Rate Using Transmission Microwave Interferometry. *Journal of Propulsion and Power* **1998**, *14* (4), 421–428. https://doi.org/10.2514/2.5318.

(5) Strand, L. D. Microwave Measurement of Solid Propellant Response Functions. 1979.

(6) Cook, M. A.; Doran, R. L.; Morris, G. J. Measurement of Detonation Velocity by Doppler Effect at Three-Centimeter Wavelength. *Journal of Applied Physics* **1955**, *26* (4), 426–428. https://doi.org/10.1063/1.1722012.

(7) FARRANDS, J. L.; CAWSEY, G. F. Microwave Observation of Detonation. *Nature* **1956**, *177* (4497), 34–35. https://doi.org/10.1038/177034a0.

(8) Krall, A. D.; Glancy, B. C.; Sandusky, H. W. Microwave Interferometry of Shock Waves. I. Unreacting Porous Media. *Journal of Applied Physics* **1993**, *74* (10), 6322–6327. https://doi.org/10.1063/1.355154.

(9) Strand, L. D.; Schultz, A. L.; Reedy, G. K. Microwave Doppler Shift Technique for Determining Solid Propellant Transient Regression Rates. *Journal of Spacecraft and Rockets* **1974**, *11* (2), 75–83. https://doi.org/10.2514/3.62012.

(10) Glancy, B. C.; Sandusky, H. W.; Krall, A. D. Microwave Interferometry of Shock Waves. II. Reacting Porous Media. *Journal of Applied Physics* **1993**, *74* (10), 6328–6334. https://doi.org/10.1063/1.355155.

(11) Bel'skii, V. M.; Mikhailov, A. L.; Rodionov, A. v.; Sedov, A. A. Microwave Diagnostics of Shock-Wave and Detonation Processes. *Combustion, Explosion and Shock Waves* **2011**, *47* (6), 639–650. https://doi.org/10.1134/S0010508211060037.

(12) Vuppuluri, V. S.; Samuels, P. J.; Caflin, K. C.; Gunduz, I. E.; Son, S. F. Detonation Performance Characterization of a Novel CL-20 Cocrystal Using Microwave Interferometry. *Propellants, Explosives, Pyrotechnics* **2018**, *43* (1), 38–47. https://doi.org/10.1002/prep.201700150.

(13) Aničin, B. A.; Jojić, B.; Blagojević, D.; Adžić, M.; Milosavljević, V. Flame Plasma and the Microwave Determination of Solid Propellant Regression Rates. *Combustion and Flame* **1986**, *64* (3), 309–319. https://doi.org/10.1016/0010-2180(86)90148-3.

(14) Zarko, V. E.; Perov, V. v.; Kiskin, A. B. Microwaves as a Tool for Energetic Materials Characterization. *40th AIAA Aerospace Sciences Meeting and Exhibit* **2002**, No. January. https://doi.org/10.2514/6.2002-190.

(15) Renslow, P. J. A Small-Scale Experiment Using Microwave Interferometry to Investigate Detonation and Shock- to-Detonation Transition in Pressed TATB. **2014**, *9*, 88.

(16) Cole, R. B. *High Pressure Solid Propellant Combustion Studies Using a Closed Bomb*; 1965.

(17) Kittell, D. E.; Mares, J. O.; Son, S. F. Using Time-Frequency Analysis to Determine Time-Resolved Detonation Velocity with Microwave Interferometry. *Review of Scientific Instruments* **2015**, *86* (4). https://doi.org/10.1063/1.4916733.

(18) Amit Sur, K. D.; Joshi, A. S.; Kaushik, T. C. VISAR Signal Analysis with an Emphasis on Ellipse Fitting. **2017**, *125002* (July).

(19) Heydemann, P. L. M. Determination and Correction of Quadrature Fringe Measurement Errors in Interferometers. **1981**, *20* (19), 3382–3384.

(20) Yaw, K. C. *Measurement of Dielectric Material Properties*; 2012.

(21) Daily, M. E. Electromagnetic Studies of Explosives at ISM (Industrial, Scientific, Medical) Frequencies, Purdue University, 2013.

(22) Dakin, T. W.; Works, C. N. Microwave Dielectric Measurements. *Journal of Applied Physics* **1947**, *18* (9), 789–796. https://doi.org/10.1063/1.1697843.

(23) Landau, L. D.; Lifshitz, E. M. Electrodynamics of Continuous Media -Volume 8 of Theoretical Physics. 1984, pp 1–474.

(24) Looyenga, H. Dielectric Constants of Heterogeneous Mixtures. *Physica* **1965**, *31* (3), 401–406. https://doi.org/10.1016/0031-8914(65)90045-5.

(25) Owen, G. P.; Thomas, J. M.; Williams, J. O. Electrical Conduction in Ammonium Perchlorate. *Journal of the Chemical Society, Faraday Transactions 1: Physical Chemistry in Condensed Phases* **1972**, *68*, 2356–2366. https://doi.org/10.1039/F19726802356.

(26) Kou, Y.; Zhou, W.; Li, B.; Dong, L.; Duan, Y. E.; Hou, Q.; Liu, X.; Cai, H.; Chen, Q.; Dang, Z. M. Enhanced Mechanical and Dielectric Properties of an Epoxy Resin Modified with Hydroxyl-Terminated Polybutadiene. *Composites Part A: Applied Science and Manufacturing* **2018**, *114* (June), 97–106. https://doi.org/10.1016/j.compositesa.2018.08.016.

(27) Neubauer, M.; Johnson, R. P.; Rimmer, R.; Elliot, T.; Stirbet, M. Rugged Ceramic Windows for RF Applications. *Proeedings of PAC* **2012**, No. November, 2089–2091.

(28) RCS Rocket Motor Components - Propellant Data, Warp-9^{TM}. p 9.

(29) Strand, L. D.; Schultz, A. L.; Reedy, G. K. *Determination of Solid-Propellant Transient Regression Rates Using a Microwave Doppler Shift Technique*; 1972. https://doi.org/10.2514/6.1972-1118.